Joint Link Scheduling and Brightness Control for Greening VLC-Based Indoor Access Networks

Sihua Shao, Abdallah Khreishah, and Issa Khalil

***Abstract*—Demands for broadband wireless access services are expected to outstrip the spectrum capacity in the near-term "spectrum crunch." Deploying additional femtocells to address this challenge is cost-inefficient due to the backhaul challenge and the exorbitant system maintenance. According to an Alcatel–Lucent report, most mobile Internet access traffic happens indoors. Leveraging power line communication and the available indoor infrastructure, visible light communication (VLC) can be utilized with a small one-time cost. VLC also facilitates the great advantage of being able to jointly perform illumination and communications, and little extra power beyond illumination is required to empower communications, thus rendering wireless access with small power consumption. In this study, we investigate the problem of minimizing total power consumption of a general multiuser VLC indoor network while satisfying users' traffic demands and maintaining an acceptable level of illumination. We utilize the column-generation method to obtain an ϵ-bounded solution. Several practical implementation issues are integrated with the proposed algorithm, including different configurations of light source and ways of resolving the interference among VLC links. Through extensive simulations, we show that our approach reduces the power consumption of the state-of-the-art VLC-based scheduling algorithms by more than 60% while maintaining the required illumination.**

***Index Terms*—Brightness control; Link scheduling; Optimization; Power consumption; Visible light communication (VLC).**

I. Introduction

The Internet has emerged as an integral part of our lives, which has gone far beyond its original use for connecting computers, and now also interconnects mobile phones, devices, and other electronic mediums. Traffic from wireless and mobile devices will exceed that from wired devices by 2019 [1]. By the same year, Wi–Fi and mobile devices will account for 66% of IP traffic. According to [2], we spend 90% of our time indoors, and 80% of the mobile Internet access traffic happens indoors [3,4]. This percentage will only increase as 54% of the cellular traffic is expected to be offloaded to Wi–Fi by 2019 [5]. It is expected that 87% of the companies would switch providers by 2019 for better indoor coverage [3].

Relying on cellular networks alone to satisfy such demand is not a cost-efficient solution because reducing the size of the cell in an arbitrary fashion introduces the backhaul challenge [6], particularly the negative profit investment in building new base stations and deploying a physical medium (e.g., copper line, Ethernet cable, microwave radio) between the base station and the last mile. This fact puts pressure on indoor networks, such as Wi–Fi networks, to support the insatiable demand for wireless Internet access. High received signal strength in indoor Wi–Fi access networks is an indicator of a fast and reliable Wi–Fi connection. However, different types of walls and other obstacles facilitate the attenuation of Wi–Fi signal strength, which will lead to the user experience of poor connectivity and slow speed. The degraded quality of service can also be caused by the non-negligible interference signal from neighboring Wi–Fi access points (APs) due to the limited bandwidth of unlicensed spectrum and the lack of coordination. To accommodate the dense and non-uniform distribution of user terminals, concurrent multi-user transmission is considered in Wi–Fi, similar to the enabled multiuser multiple-input and multiple-output (MU-MIMO) in long-term evolution (LTE). However, a huge effort is required to standardize a new mode of simultaneous transmissions to multiple users that must remain backwards compatible. Moreover, the complexity of linear MIMO equalizers scales by a factor of N^3, where N is the number of antennas. Due to these standardization, scalability, and complexity issues, and due to the increasing demand for Wi–Fi, there is rationale to consider other wireless mediums.

To alleviate the problems of system construction and maintenance, and to enhance spectrum reusability, innovative approaches need to be adopted, among which visible light communication (VLC) is a complementary candidate. The VLC microcells can supplement RF cells in areas such as apartment complexes, coffee shops, and office spaces where device density and data demand are at their highest. One benefit of densely distributed VLC microcells is that interference between AP layout controlled by a local entity and controlled by neighboring entities is negligible (i.e., because of the short transmission range and obstruction by

Manuscript received August 20, 2015; revised December 6, 2015; accepted January 4, 2016; published 0, 0000 (Doc. ID 248152).

Sihua Shao (e-mail: ss2536@njit.edu) and Abdallah Khreishah are with the Department of Electrical and Computer Engineering, New Jersey Institute of Technology, Newark, New Jersey 07102, USA.

Issa Khalil is with the Qatar Computing Research Institute, Hamad bin Khalifa University, Doha, Qatar.

http://dx.doi.org/10.1364/JOCN.99.099999

 © 2016 Optical Society of America

walls). In this way, provisioning of the VLC network can be evaluated locally and dynamic control (e.g., resource allocation, beam adaptation, handover) can be locally coordinated. The most attractive feature of VLC is utilizing the available indoor infrastructure in terms of power over Ethernet (PoE) and power line communications (PLC). PLC has been able to achieve data rates of 1 Gbps [7,8] and only requires adapters to perform communications. PoE is widely used to control lighting level (without communications) as in the light as a service (LaaS), which is [9] provided by Cisco. These facts enable the VLC systems implementation in practice with a small one-time cost based on the available indoor infrastructure (i.e., backhaul links and light sources). As a complementary approach to the existing wireless RF solutions, VLC is expected to relieve the pressure on the crowded radio spectrum and become a promising broadband wireless access candidate to resolve the "spectrum crunch" problem [10].

For an indoor environment, whenever communication is needed, *lighting is also needed most of the time*. It is worth noting that VLC consumes additional power when performing communication functionality in addition to illumination, which is also introduced in [11]. The amount of additional power consumed by data transmission depends on the driver circuitry, and we will demonstrate this power efficiency by a factor in Section III. Along with the development of the driver, VLC is expected to operate on a small energy budget by jointly performing lighting and Internet access.

For upper layers in multiuser scenarios, [12] and [13] consider link scheduling algorithms to serve multiple users based on multiple VLC links with no power efficiency guarantees. The work in [12] relies on a simple impractical assumption to measure the illumination using the average SNR distribution. The work in [14] proposes an energy-efficient brightness control and data transmission scheme for VLC. However, the scheme can only be applied to the single user scenario, and only the optical power is taken into account when minimizing the power consumption.

In this paper, we investigate the problem of optimizing total power consumption of a general multiuser VLC indoor network while satisfying the traffic demands and illumination requirements. A novel algorithm is proposed to efficiently obtain a practical ϵ-bounded solution. Our contributions are summarized as follows:

- **Minimizing the total power consumption for a general multiuser VLC indoor network**: Taking the users' traffic demand and the illumination requirement of an entire horizontal space into account, the total power consumption of a general multiuser VLC indoor network is optimized via a novel efficient and practical algorithm.
- **Effectively model the level of interference among VLC links**: Based on the proposed algorithm, an effective interference management approach is verified by extensive simulation results.
- **Design of a novel structure of a light source**: An innovative configuration of a light source is proposed and analyzed and compared with two other common configurations in terms of total power consumption.
- **Validating the power efficiency and illumination satisfaction**: Extensive simulation results reveal that our proposed link scheduling algorithm can provide around 60% and 80% saving in power consumption compared to two VLC-based solutions, and the illumination distribution obtained by our proposed algorithm can always satisfy the requirements.

II. Related Work

Much effort has been put toward the VLC indoor network; however, most efforts do not provide comprehensive consideration of the illumination and communication or only focus on limited aspects. Even though one of them [12] proposes a framework for configuring VLC indoor networks with adjustable LED beam angle and beam width, the link scheduling algorithm has no power efficiency guarantees and the framework relies on a simple impractical assumption to measure the illumination using the average SNR distribution.

The LED angle tuning issue is also studied in [15], which only presents the heuristic simulation results of the average SNR distribution without considering illumination. For the cooperation among VLC cells, the work in [16] presents an elaborate study on the bandwidth efficiency of four different VLC cell formations. However, in the cooperative load balancing approach, the users' traffic demand is not considered. The merging VLC cell approach is also studied in [13], which has not taken the illumination into account. In [17], an optimal Lambertian order algorithm is proposed. To maximize the VLC cell boundary signal strength, an optimal Lambertian order can be found by calculating the first-order derivative of the VLC path loss model. Whereas the illumination and multiple user scenario are not considered in this work. The work in [18] introduces the concept of DC and AC optical power without considering overall power consumption optimization and the distribution of illumination. In [14], the authors investigate the energy efficiency for only optical power with brightness control and data transmission in VLC networks. Three power levels of the subcarrier pulse position modulation scheme are utilized as the variables to perform the power consumption optimization. Nonetheless, in their optimization constraints, the brightness control is only applied to the location of the user, which is not practicable. A multi-transceiver optical wireless spherical structure is proposed in [19]. The spherical optical antenna is tessellated with multiple LEDs to enable the beam angle diversity. However, this design does not carefully consider the illumination functionality of LEDs. The transverse line-of-sight of the spherical optical antenna may produce glaring in some specific scenarios. Several brightness control methods have been introduced in [20]. The PWM and DC bias are two predominant approaches for dimming control. A room division multiplexing-based VLC network is proposed in [21], while, in our work, the concept of space division multiplexing is manifested by adjusting the Lambertian order.

III. System Model

A. Access System Model

Consider a visible light access system model (Fig. 1) comprising $\mathcal{V} = \{1, 2, \ldots, i, \ldots, V\}$ VLC APs, $\mathcal{M} = \{1, 2, \ldots, j, \ldots, M\}$ user terminals (UTs), and $\mathcal{W} = \{1, 2, \ldots, b, \ldots, W\}$ available channels with different bandwidths implemented by frequency division multiplexing (FDM). For instance, assume we have three VLC APs and the −3 dB cut-off frequency of each VLC AP is 30 MHz; then, the channel bandwidth allocated to each VLC AP can be 9 MHz with 2 MHz as a guard band between each pair of adjacent channels. The carrier frequency of each channel is at 5, 15, and 25 MHz, respectively. Note that the frequency division (MHz level) discussed here is different from wavelength division (THz level), which is implemented in the visible light spectrum. The bandwidth of channel b is denoted by B^b. We also denote the set of transmitters on VLC AP $i \in \mathcal{V}$ by $Tx_i = \{1, 2, \ldots, m, \ldots, |Tx_i|\}$, where $|Tx_i|$ is the number of transmitters on VLC AP i, and the set of receivers on UT $j \in \mathcal{M}$ by $Rx_j = \{1, 2, \ldots, n, \ldots, |Rx_j|\}$, where $|Rx_j|$ is the number of receivers on UT j. We assume the UT j has a throughput requirement of $\mathcal{R}_j$.

A recent measurement study [22] on traces of 3785 smart phone users from 145 countries over a four-month period shows that the ratio of Wi–Fi download traffic to its upload traffic is 20:1. Therefore, in this work, we mainly consider the power consumption for the downlink data transmission. Regarding the uplink issue in VLC networks, a hybrid Wi–Fi VLC Internet access system (VLC downlink and Wi–Fi uplink) is presented in our earlier work [23–27].

B. Communication

Optical modulation is performed by varying the forward current of the light source. The output optical power changes proportionally to the modulated forward current. The increase in total power consumption (including the power consumed by the modulator) is mainly due to the switching loss in the driver circuitry at high speed (AC current for modulation). Such behavior is observed in our preliminary experimental results and the results in [28]. Here, we denote a peak-to-peak optical signal strength (generated from AC current) by P_{AC} and its average value by $P_{\mathrm{AC,Avg}}$. Note that the P_{AC} will be used later in this section to estimate the channel capacity by the Shannon equation. By utilizing the peak optical power that is constrained by the type of light source, the Shannon capacity acts as an upperbound for the channel capacity regardless of which specific modulation scheme is used.

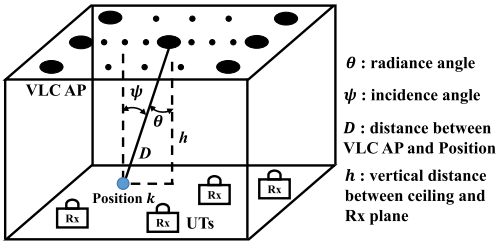

Fig. 1. System model for multiuser VLC indoor network.

C. Illuminance

Consider a horizontal user plane comprising $\mathcal{K} = \{1, 2, \ldots, k, \ldots, K\}$ positions, and each position requires an illumination level in the range of E_k^L and E_k^U. The illumination level of ambient light at position k is denoted by E_k^{Am}.

The illumination level at a given location depends on the average optical power received. This can be generated by the DC and AC current. We denote an optical DC power (generated from DC current) by P_{DC}, which is responsible for compensating the average AC power in order to meet the illumination demands.

The DC component does not require a current switching process. This switching process reduces the efficiency of the driver circuit and light source by consuming more power. Thus, for the transmitter m of the ith VLC AP, we denote $\eta_{\mathrm{AC}}^{i,m}$ and $\eta_{\mathrm{DC}}^{i,m}$ as the wall plug efficiency factors (i.e., the ratio of the optical power consumption to the electrical power consumption) for AC and DC optical power, respectively, where $\eta_{\mathrm{AC}}^{i,m}$ is generally smaller than $\eta_{\mathrm{DC}}^{i,m}$.

The illuminance represents the level of brightness of the illuminated surface. A horizontal illuminance E_k [lux] at position k can be given [14] as $E_k = \sum_{\substack{i \in \mathcal{V} \\ m \in Tx_i}} (P_{\mathrm{DC}}^{i,m} g_{i,k,m}^{\mathrm{DC}} + P_{\mathrm{AC,Avg}}^{i,m} g_{i,k,m}^{\mathrm{AC}}) \rho$, where $P_{\mathrm{DC}}^{i,m}$ and $P_{\mathrm{AC,Avg}}^{i,m}$ denote the generated DC and average AC optical power from the transmitter m of the ith VLC AP, respectively, ρ [lm/W] is the luminosity efficacy, and $g_{i,k,m}^{\mathrm{DC}}$ and $g_{i,k,m}^{\mathrm{AC}}$ are given as follows:

$$g_{i,k,m}^{\mathrm{DC}} = \frac{ml_{\mathrm{DC}} + 1}{2\pi D^2} \cos^{ml_{\mathrm{DC}}}(\theta_{\mathrm{DC}}) \cos(\psi),$$

$$g_{i,k,m}^{\mathrm{AC}} = \frac{ml_{\mathrm{AC}} + 1}{2\pi D^2} \cos^{ml_{\mathrm{AC}}}(\theta_{\mathrm{AC}}) \cos(\psi),$$

where ml is the Lambertian order ($ml = -\ln 2 / \ln(\cos \theta_{1/2})$, $\theta_{1/2}$ is the semi-angle at half-power), (in Fig. 1) D is the distance between VLC AP i and position k, θ is the radiance angle, and ψ is the incidence angle. Note that, the ml and θ of the DC and AC powered source could be different, which will be discussed in detail in Section VI.

D. Channel Capacity, Interference, and Noise

From [29], the received optical intensity via a line-of-sight (LOS) path is about 30 times higher than that via the first reflective path. Because LOS paths are typically feasible, in this paper, we only consider the LOS links. The LOS channel gain between VLC AP i, using transmitter m, and UT j, using receiver n, denoted by $H_{ij,mn}$, is illustrated in [29]. The LOS channel DC gain can be expressed as

$$H = \begin{cases} \frac{(ml+1)A}{2\pi D^2}\cos^{ml}(\theta)\cos(\psi)T_s(\psi)g(\psi), & 0 \le \psi \le \Psi_c \\ 0, & \psi > \Psi_c \end{cases},$$

where ml is the Lambertian order ($ml = -\ln 2/\ln(\cos\theta_{1/2})$, $\theta_{1/2}$ is the semi-angle at half-power), A is the detector physical area of the photodiode (in Fig. 1), D is the distance between a transmitter and a receiver, θ is the radiance angle, ψ is the incidence angle, $T_s(\psi)$ is the gain of an optical filter, and $g(\psi)$ is the gain of an optical concentrator. Ψ_c denotes the FOV of a receiver. The optical concentrator $g(\psi)$ can be given [29] as

$$g(\psi) = \begin{cases} \frac{n^2}{\sin^2\Psi_c}, & 0 \le \psi \le \Psi_c \\ 0, & \psi > \Psi_c \end{cases},$$

where n denotes the refractive index.

It is worth noting that the gain of the VLC channel highly depends on the strict alignment between VLC transceivers. In contrast with the omnidirectional Wi–Fi channel, the potential movement and rotation of user terminals will lead to severe degradation of the VLC channel gain. Nevertheless, according to [4], the majority of mobile data usage—close to 80%—is indoor and nomadic, rather than truly mobile. For nomadic situations, the location of the terminal may change, but the terminal is stationary while it is in use. Unless the user devices change their locations and orientations while receiving or transmitting data packets, the VLC channel condition will not suffer the severe degradation. Thus, we focus on scenarios in which the UTs' location remain fixed while in use, where the channel gain of VLC is more stable than that of Wi–Fi [30].

The Gaussian noise of the optical wireless channel consists of the shot noise (stems from the received optical power) and the thermal noise (stems from the receiver's circuitry). Increasing the transmitted optical power increases the noise level at the receiver. However, if the modulation bandwidth is large (above 50 MHz) and the optical power level is low (below 20 W) as is the case with most VLC APs and VLC front-ends [31], the thermal noise would dominate the shot noise [29]. With fixed gain of the receiver, the thermal noise is essentially independent of the ambient light and signal strength while the shot noise is not. Our experimental results [24] have validated this behavior even in outdoor settings. Therefore, a constant variance of Gaussian noise can be assumed.

Typically, there are two major interference models for the wireless networks [32]: physical model and protocol model. Under the physical model, the link capacity depends on the signal-to-interference-plus-noise ratio at the receiver side. It is an accurate representation of real scenarios, but it is computationally difficult to work with. On the other hand, the protocol model only considers the pairwise interference relationship among the links. With the protocol model, the interference among individual VLC links can be modeled through the use of a conflict graph [33]. The approach works as follows. Each receiver on a UT or each transmitter on a VLC AP is represented by a vertex in a graph. If a transmitter can transmit to a receiver on a given channel, an edge is drawn between the two vertices representing the transmitter and the receiver. The conflict graph is then constructed, such that each edge in the original graph is represented by a vertex in the conflict graph. An edge in the conflict graph is drawn between two vertices if the corresponding edges in the original graph interfere with each other. An interference constraint (addressed in details in the next section) represents the fact that, for a successful transmission (i.e., vertex in the conflict graph), none of those vertices (i.e., links in the original graph) connected by an edge in the conflict graph are active at the same time. Based on this interference constraint, the link capacity depends on the signal-to-noise ratio (SNR) under the protocol model.

Given a link with bandwidth B^b, based on the Shannon–Hartley theorem [34], the maximum link capacities C when VLC AP i, using transmitter m, transmits data to UT j, using receiver n, on channel b, in two interference models are given [35] by

$$C^b_{ij,mn}(\text{Protocol}) = B^b \times \log_2\left(1 + \frac{(\gamma H_{ij,mn}P^{i,m}_{\text{AC}})^2}{N}\right), \quad (1)$$

$$C^b_{ij,mn}(\text{Physical}) = B^b \times \log_2\left(1 + \frac{(\gamma H_{ij,mn}P^{i,m}_{\text{AC}})^2}{(\gamma P_I)^2 + N}\right), \quad (2)$$

where γ is the detector responsivity, P_I is the summation of the interference optical power, and N is the variance of noise. The main notations are summarized in Table I.

IV. Problem Formulation

We investigate the minimum power consumption problem for a multiuser VLC indoor network by joint link scheduling and illuminating. For a conflict graph under the protocol model, an *independent set* (IS) $\mathcal{I}$ is defined as a set of vertices in the conflict graph (i.e., links in the original graph) such that none of them are connected by an edge [33].

Suppose all the ISs are known and the set of all ISs is denoted as $\mathcal{Q} = \{\mathcal{I}_1, \mathcal{I}_2, \ldots, \mathcal{I}_q, \ldots, \mathcal{I}_{|\mathcal{Q}|}\}$. In order to ensure the successful transmissions in each IS, at any given time, only one IS should be active. We define ω_q as the fraction of the time during which the qth IS is active. Therefore, we have

$$\sum_{1\le q\le|\mathcal{Q}|}\omega_q \le 1, \omega_q \ge 0. \quad (3)$$

An integer variable is defined as follows: $x^{q,b}_{ij,mn}$ is equal to 1 if VLC AP i, using transmitter m, transmits to UT j, using receiver n, on channel b, in $\mathcal{I}_q$, and equal to 0 otherwise.

Recall that the jth UT's throughput requirement is $\mathcal{R}_j$. In order to meet the traffic demands of users, the following set of constraints needs to be satisfied:

$$\sum_{1\le q\le|\mathcal{Q}|}\omega_q \sum_{\substack{i\in\mathcal{V},b\in\mathcal{W}\\ m\in Tx_i, n\in Rx_j}} C^b_{ij,mn}x^{q,b}_{ij,mn} \ge \mathcal{R}_j \qquad (\forall\, j \in \mathcal{M}), \quad (4)$$

where $C^b_{ij,mn}$ is calculated by Eq. (1).

TABLE I
SYMBOL DEFINITION

$\mathcal{Q}$	Set of all ISs
$\tilde{\mathcal{Q}}$	Set of observed ISs
$\mathcal{I}_q$	The qth IS
ω_q	Time fraction scheduled for the qth IS
$\mathcal{M}$	Set of UTs
$\mathcal{V}$	Set of VLC APs
$\mathcal{K}$	Set of positions
$\mathcal{W}$	Set of available channels
Tx_i	Set of transmitters on VLC AP i
Rx_j	Set of receivers on UT j
$x_{ij,mn}^{q,b}$	Integer value (0 or 1) denoting whether the link from the mth transmitter of the ith VLC AP to the nth receiver of the jth UT using channel b is active or not
$P_{\text{AC,Avg}}(\mathcal{I}_q)$	Total AC power consumption of the qth IS
$P_{\text{DC}}(\mathcal{I}_q)$	Total DC power consumption of the qth IS
$P_{\text{AC}}^{i,m}$	Static peak-to-peak signal strength of the mth transmitter of the ith VLC AP
$P_{\text{AC,Avg}}^{i,m}$	Average AC optical power consumption of the mth transmitter of the ith VLC AP
$P_{\text{DC}}^{i,q,m}$	Dynamic DC optical power consumption of the mth transmitter of the ith VLC AP in the qth IS
$P_{\max}^{i,m}$	Maximum optical power of the mth transmitter of the ith VLC AP
$g_{i,k,m}^{\text{DC}}/g_{i,k,m}^{\text{AC}}$	DC/AC optical power gain
E_k^{Am}	Illuminance level of ambient light at the kth position
E_k^L/E_k^U	Lower bound/upper bound of the horizontal illuminance level at the kth position
$\mathcal{C}_{ij,mn}^b$	Maximum link capacity when VLC AP i, using transmitter m, transmits data to UT j, using receiver n, on channel b
$\mathcal{R}_j$	jth UT's throughput requirement
λ_j	Solution of the dual problem for the jth UT
$\mathcal{T}_{ij,mn}^b$	Set of links that interfere the transmission from the mth transmitter of the ith AP to the nth receiver of the j_{th} UT on channel b
$\eta_{\text{AC}}^{i,m}/\eta_{\text{DC}}^{i,m}$	TAC/DC efficiency factor denoting the ratio of electrical power consumption to optical power consumption of the mth transmitter of the ith VLC AP

Denote $P_{\text{DC}}^{i,q,m}$ as the ith VLC AP's DC optical power consumption of the transmitter m in the qth IS and $P_{\text{AC}}^{i,m}$ as the fixed peak-to-peak signal strength of the ith VLC AP's transmitter m. For one VLC transmitter, the summation of P_{AC} and P_{DC} cannot exceed the maximum optical power $P_{\max}$. Thus, we have

$$P_{\text{DC}}^{i,q,m} + \sum_{j\in\mathcal{M},b\in\mathcal{W},n\in Rx_j} P_{\text{AC}}^{i,m} x_{ij,mn}^{q,b} \le P_{\max}^{i,m} \quad (\forall\, i\in\mathcal{V}, \forall\, m\in Tx_i, 1\le q\le|\mathcal{Q}|). \tag{5}$$

Recall that, at position k, the minimum and maximum illuminance thresholds are E_k^L and E_k^U, respectively, and the illuminance level of ambient light is E_k^{Am}. The summation of the LED lighting and the ambient lighting needs to be within the range $[E_k^L, E_k^U]$. Therefore, we have the following illumination constraints:

$$E_k^U \ge \sum_{\substack{i\in\mathcal{V},j\in\mathcal{M},b\in\mathcal{W},\\ m\in Tx_i,n\in Rx_j}} (P_{\text{AC,Avg}}^{i,m} x_{ij,mn}^{q,b} g_{i,k,m}^{\text{AC},q} + P_{\text{DC}}^{i,q,m} g_{i,k,m}^{\text{DC}})\rho + E_k^{Am} \ge E_k^L \quad (\forall\, k\in\mathcal{K}, 1\le q\le|\mathcal{Q}|). \tag{6}$$

The reason for adding the superscript q to the AC optical power gain is that the Lambertian order or the radiance angle of the AC powered source on each VLC transmitter may be varied in different ISs. This condition will be demonstrated in detail in Section VI.

Given the link scheduling in each IS, the illuminance distribution from the average AC optical power can be obtained. Therefore, to satisfy the maximum power constraint in Eq. (5) and the illumination constraint in Eq. (6), we can compute the optimal $P_{\text{DC}}^{i,q,m}$ for each VLC transmitter in each IS. Denote $P_{\text{AC,Avg}}(\mathcal{I}_q)$ and $P_{\text{DC}}(\mathcal{I}_q)$ as the total AC and DC power consumption of the qth IS, respectively. The optimal solution of our algorithm might result in $\sum_{1\le q\le|\mathcal{Q}|}\omega_q < 1$; this means that the data transmission will be completed within the $\sum_{1\le q\le|\mathcal{Q}|}\omega_q$ fraction of time. However, the illumination is always needed. Let $P_{\text{illumi}}^{\min}$ represent the minimum total power consumption when all the VLC APs only perform illumination. This means that, during the $(1-\sum_{1\le q\le|\mathcal{Q}|}\omega_q)$ fraction of time, the power consumption is $P_{\text{illumi}}^{\min}$. Therefore, the total power consumption optimization problem can be formulated as follows:

$$\min_{\omega_q} \sum_{1\le q\le|\mathcal{Q}|} \omega_q[P_{\text{AC,Avg}}(\mathcal{I}_q) + P_{\text{DC}}(\mathcal{I}_q)] + \left(1 - \sum_{1\le q\le|\mathcal{Q}|}\omega_q\right) P_{\text{illumi}}^{\min}$$
$$\text{s.t. } (3), (4)$$

where

$$P_{\text{AC,Avg}}(\mathcal{I}_q) + P_{\text{DC}}(\mathcal{I}_q) = \sum_{\substack{i\in\mathcal{V},j\in\mathcal{M},b\in\mathcal{W},\\ m\in Tx_i,n\in Rx_j}} \left(\frac{1}{\eta_{\text{AC}}^{i,m}} P_{\text{AC,Avg}}^{i,m} x_{ij,mn}^{q,b} + \frac{1}{\eta_{\text{DC}}^{i,m}} P_{\text{DC}}^{i,q,m}\right).$$

This problem aims to minimize the total power consumption by satisfying the traffic demands, illumination requirement and maximum optical power constraint of each transmitter. Given that all the ISs satisfying constraints in Eqs. (5) and (6), the formulated optimization problem is a linear programming problem due to the fact that $x_{ij,mn}^{q,b}$ is known *a priori* for each IS. We call this problem the *master problem* (MP). The solution to the MP is to find the optimal values of ω_q $(1\le q\le|\mathcal{Q}|)$. After the scheduling algorithm finds out the fraction of time that each independent set (i.e., set of links that can be active simultaneously) is active, the independent sets will be scheduled in a round-robin basis. As shown in Fig. 2, based on the conflict graph (left figure), an example of the time scheduling of the five links is presented (right figure). In the first time slot, the first independent set, including link 1 and link 2, occupies the first time fraction ω_1; the second

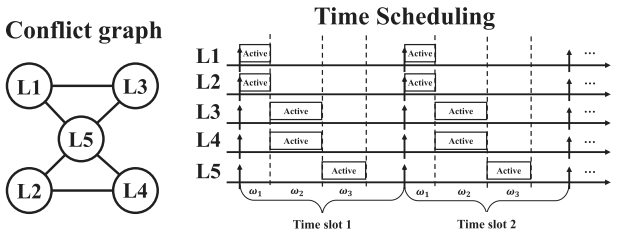

Fig. 2. Example of round-robin based time scheduling.

independent set, including link 3 and link 4, occupies the second time fraction ω_2; the last independent set, including only link 5, occupies the third time fraction ω_3. The scheduling in the first time slot will be repeated in the following time slots until the network pattern changes. In the next section, we will introduce the challenges of solving the MP and our solution methodology.

V. Solution Methodology

A. Challenges of Solving the MP

To efficiently solve the MP, there are two main challenges: (1) Although the MP is a linear programming problem if all the ISs are given, the IS decision problem itself is NP-complete [33]; hence, it is believed that there is no efficient algorithm for solving it. (2) Even if all the ISs are given, the number of ISs and corresponding variables increases exponentially as the number of links increases. Therefore, the complexity of solving the MP will be extremely high when the network is very large. We propose a column-generation-based ϵ-bounded algorithm to resolve these challenges.

B. Column Generation

Column generation [36] is an efficient algorithm for solving large-scale (i.e., the number of variables is large) linear programming problems. Even though the MP has a large number of variables, only a small subset of them will be nonzero (basis variables) in the optimal solution. Based on this observation, rather than adding all the variables in the MP, column generation only generates the variables with the highest potential to enhance the objective function. In particular, the large MP is split into two smaller and simpler problems: the *restricted master problem* (RMP) and the *pricing problem* (PP). The RMP only includes an initial subset of variables in the MP, and the PP is a new optimization problem assigned to find a variable or a column (i.e., independent set), which has the most negative reduced cost (i.e., decrease of the objective value). The process works iteratively as follows: the RMP is solved, and its optimal and dual optimal solutions are obtained; the PP utilizes the dual optimal solution of the RMP to identify the column with the most negative reduced cost and adds it into the RMP to reoptimize the RMP. The process continues until the objective value of the PP is non-negative. If the PP returns a non-negative solution, the solution of the RMP is the optimal solution to the MP.

Instead of considering the set $\mathcal{Q}$ of all the ISs, the RMP starts with an initial set $\tilde{\mathcal{Q}}$ of ISs (called observed ISs). A simple method of selecting the initial ISs is to place only one active link in each of them. Hence, the RMP is formulated as follows:

$$\min_{\omega_q} \sum_{1\le q\le|\tilde{\mathcal{Q}}|} \omega_q[P_{\mathrm{AC,Avg}}(\mathcal{I}_q)+P_{\mathrm{DC}}(\mathcal{I}_q)] + \left(1-\sum_{1\le q\le|\tilde{\mathcal{Q}}|}\omega_q\right)P^{\min}_{\mathrm{illumi}}$$
$$\text{s.t.} \sum_{1\le q\le|\tilde{\mathcal{Q}}|} \omega_q \sum_{\substack{i\in\mathcal{V},b\in\mathcal{W},\\ m\in Tx_i,n\in Rx_j}} \mathcal{C}^b_{ij,mn}x^{q,b}_{ij,mn} \ge R_j \qquad (\forall\, j\in\mathcal{M}),$$
$$\sum_{1\le q\le|\tilde{\mathcal{Q}}|} \omega_q \le 1, \omega_q \ge 0,$$

where $P_{\mathrm{DC}}(\mathcal{I}_q)$ $(1\le q\le|\tilde{\mathcal{Q}}|)$ can be computed optimally by satisfying the maximum power constraint in Eq. (5) and the illumination constraint in Eq. (6). The objective and constraint of the RMP are almost the same as those of the MP. The only difference is that the number of ISs considered in the RMP is much less than that in the MP. This means that the number of variables in the RMP is much less than that in the MP, which lead to a lower complexity of initially solving the problem.

After solving the RMP, the primal optimal solution and the Lagrangian dual optimal solution can be obtained. Because the ISs in the RMP are only a subset of the ISs in the MP (i.e., $\tilde{\mathcal{Q}}\subseteq\mathcal{Q}$), the primal optimal solution of the RMP can be regarded as an upper bound of the optimal solution of the MP. Adding another column, which does not exist in the RMP, may reduce the upper bound and improve the objective function. Therefore, the PP is responsible for generating a column with the most negative reduced cost.

For an IS that has not been observed (i.e., included in the RMP), the PP needs to determine whether the reduced cost of the IS is negative or not. Referring to [36], the reduced cost of $\mathcal{I}_q$ can be calculated as $c_r(\mathcal{I}_q)-P^{\min}_{\mathrm{illumi}}$, where

$$c_r(\mathcal{I}_q) = \sum_{\substack{i\in\mathcal{V},j\in\mathcal{M},b\in\mathcal{W},\\ m\in Tx_i,n\in Rx_j}} \left(\frac{1}{\eta^{i,m}_{\mathrm{AC}}}P^{i,m}_{\mathrm{AC,Avg}}x^{q,b}_{ij,mn} + \frac{1}{\eta^{i,m}_{\mathrm{DC}}}P^{i,q,m}_{\mathrm{DC}}\right) - \sum_{j\in\mathcal{M}}\lambda_j \sum_{\substack{i\in\mathcal{V},b\in\mathcal{W},\\ m\in Tx_i,n\in Rx_j}} \mathcal{C}_{ij,mn}x^{q,b}_{ij,mn},$$

where λ_j is the Lagrangian dual optimal solution for the jth UT. To find the $\mathcal{I}_q$ with the most negative reduced cost, the objective of the PP is to minimize $c_r(\mathcal{I}_q)-P^{\min}_{\mathrm{illumi}}$.

Regarding the constraints of the PP, under the protocol model, we denote $\mathcal{T}^b_{ij,mn}$ as the set of links that interfere with the transmission from the ith AP, using transmitter m, to the jth UT, using receiver n, on channel b. Thus, we have

$$x^b_{ij,mn} + \sum_{pq,uv\in\mathcal{T}_{ij,mn}} x^b_{pq,uv} \le 1 \qquad (\forall\, i\in\mathcal{V},\forall\, j\in\mathcal{M},\forall\, m\in Tx_i,\forall\, n\in Rx_j). \tag{7}$$

In addition, the total number of transmitting links at VLC AP i and receiving links at UT j should be no larger than $|Tx_i|$ and $|Rx_j|$, respectively, which means

$$\sum_{\substack{j\in\mathcal{M},b\in\mathcal{W},\\ m\in Tx_i,n\in Rx_j}} x^b_{ij,mn} \le |Tx_i| \qquad (\forall\, i\in\mathcal{V}), \tag{8}$$

$$\sum_{\substack{i\in\mathcal{V},b\in\mathcal{W},\\ m\in Tx_i,n\in Rx_j}} x^b_{ij,mn} \le |Rx_j| \qquad (\forall\, j\in\mathcal{M}). \tag{9}$$

Besides, a transmitter of a VLC AP cannot transmit to multiple UTs and a receiver of a UT cannot receive from multiple VLC APs due to interference. Therefore, we obtain

$$\sum_{j\in\mathcal{M},b\in\mathcal{W},n\in Rx_j} x^b_{ij,mn} \le 1 \qquad (\forall\, i\in\mathcal{V},\forall\, m\in Tx_i), \tag{10}$$

$$\sum_{i\in\mathcal{V},b\in\mathcal{W},m\in Tx_i} x^b_{ij,mn} \le 1 \qquad (\forall\, j\in\mathcal{M},\forall\, n\in Rx_j). \tag{11}$$

It is worth noticing that, in contrast to RF communication, the optical signal propagation may not be isotropic from the perspective of the UT plane (e.g., the central luminous flux is not vertical to the horizontal UT plane), and also the orientation and field of view (FOV) of the VLC receiver can be tuned in order to receive signals from a specific direction and a small range. Thus, using the same channel, a transmitter of a VLC AP can transmit to multiple UTs, and a UT can receive from multiple VLC APs.

Assembling together the constraints of power and brightness control with the above constraints, the PP can be formulated as follows:

$$\begin{aligned}
&\min_{\mathcal{I}_q\in\mathcal{Q}\setminus\tilde{\mathcal{Q}}} c_r(\mathcal{I}_q) - P^{\min}_{\text{illumi}}\\
&\quad \text{s.t. } (7),(8),(9),(10),(11)\\
&P^{i,m}_{\text{DC}} + \sum_{j\in\mathcal{M},b\in\mathcal{W},n\in Rx_j} P^{i,m}_{\text{AC}} x^b_{ij,mn} \le P^{i,m}_{\max}\\
&\quad (\forall\, i\in\mathcal{V},\forall\, m\in Tx_i)\\
&E^U_k \ge \sum_{\substack{i\in\mathcal{V},j\in\mathcal{M},b\in\mathcal{W}\\ m\in Tx_i,n\in Rx_j}} (P^{i,m}_{\text{DC}} g^{\text{DC}}_{i,k,m} + P^{i,m}_{\text{AC,Avg}} x^b_{ij,mn} g^{\text{AC}}_{i,k,m})\rho\\
&\qquad + E^{Am}_k \ge E^L_k \qquad (\forall\, k\in\mathcal{K})\\
&x^b_{ij,mn}\in\{0,1\}\\
&\quad (\forall\, i\in\mathcal{V},\forall\, j\in\mathcal{M},\forall\, m\in Tx_i,\forall\, n\in Rx_j,\forall\, b\in\mathcal{W})
\end{aligned}$$

where $P^{i,m}_{\text{DC}}$ and $x^b_{ij,mn}$ are the variables. The PP aims to find an IS with the minimum reduced cost by constraining the links in that IS to satisfy the conflict graph constraints, illumination requirement, and maximum optical constraint of each VLC transmitter.

The RMP and the PP are solved in an iterative way, until the PP returns a non-negative reduced cost. However, because the size of $\mathcal{Q}$ could be huge, it might take a long time to reach the optimal solution. Therefore, instead of finding the optimal solution, we propose an ϵ-bounded termination condition to find a satisfactory ϵ-bounded solution.

C. ϵ-Bounded Termination Condition

Let z^* denote the optimal result of the MP and z^u denote the optimal result of the RMP (upper bound on z^*); when $\kappa \ge \sum_{1\le q\le|\mathcal{Q}|}\omega_q$ holds for the optimal solution of the MP, the z^u cannot be reduced more than κ times the most negative reduced cost c^*_r [37]:

$$z^u + \kappa c^*_r \le z^* \le z^u.$$

Denote $z^l = z^u + \kappa c^*_r$ as the lower bound on z^* and the following lemma can be proved.

Lemma 1: Define ϵ as $0 \le \epsilon < 1$. The optimal solution of the RMP $z^u \le (1+\epsilon)z^*$, if $z^u/z^l \le 1+\epsilon$.

Proof: If $z^u/z^l \le 1+\epsilon$, then $z^u \le (1+\epsilon)z^l \le (1+\epsilon)z^*$. Hence, by setting a termination condition in the column-generation-based algorithm, when the algorithm terminates, the obtained solution achieves an objective value within $(1+\epsilon)$ of the optimal. ∎

Based on the ϵ-bounded termination condition, the iteration of column generation can be terminated when $c^*_r \ge 0$ or $z^u/z^l \le 1+\epsilon$. Note that, if we set $\epsilon = 0$, then the column-generation algorithm will obtain the optimal solution of the MP.

D. Reality Check

Although the column-generation-based ϵ-bounded algorithm is capable of efficiently finding the ϵ-bounded solution of the MP, the feasibility of the protocol model solution is doubtful. Under the protocol model, the impact of some nonzero interfering links are neglected, which may lead to overestimation of the achievable link capacity. Thus, the power consumption solution (under the protocol model) of the MP may be lower than the real power consumption in practice. To investigate the practical objective value of the MP, a validation process called "reality check" is introduced in [38]. Note that, in [38], the "reality check" process is neither integrated with the column-generation algorithm nor applied to evaluate the real power consumption.

Because the protocol model solution of the RMP includes all the ISs with nonzero ω_q, the link scheduling (i.e., which link is active and which link is idle) of each of those ISs can be known. Hence, the actual achievable capacity of each active link can be recomputed by Eq. (2). The "reality check" process consists of two steps: 1) recompute the actual link capacity by Eq. (2) for the protocol model solution of the RMP, and 2) substitute the recomputed link capacity into the RMP and solve the constraint-updated RMP to obtain a feasible solution of power consumption. In particular, we take the link scheduling shown in Fig. 2 as an example. Link 1 and link 2 are assigned in the first independent set because they are "not conflicted" with each other in the conflict graph. However, the "not conflicted" here does

not mean that the interference between link 1 and link 2 is zero. Assume the protocol model's link capacities (i.e., when only the corresponding link is active and all other nonzero interference links are idle) of link 1 and link 2 are both 10 Mbps, and the solution ω_1 based on these two link capacities is 0.1 s. When the nonzero interference between link 1 and link 2 is taken into account, the physical model's link capacities of link 1 and link 2 should be both less than 10 Mbps, which means that the time fraction ω_1 allocated to the first independent set needs to be increased above 0.1 s. Therefore, we need to solve the constraint-updated RMP to figure out the feasible solutions (i.e., $\omega_q's$). The column-generation-based ϵ-bounded algorithm with reality check is summarized in Algorithm 1.

Algorithm 1 Column-generation-based ϵ-bounded algorithm with reality check

Input: Initial independent sets $\tilde{\mathcal{Q}}$, traffic demands $\mathcal{R}_j$, interference set of each link $\mathcal{T}^b_{ij,mn}$, protocol model link capacity $\mathcal{C}^b_{ij,mn}$, optical signal strength $P^{i,m}_{\mathrm{AC}}$, maximum power consumption $P^{i,m}_{\max}$, termination condition factor ϵ, gains of AC and DC optical power $g^{\mathrm{AC}}_{i,k,m}$ and $g^{\mathrm{DC}}_{i,k,m}$, wall plug efficiency factors $\eta^{i,m}_{\mathrm{AC}}$ and $\eta^{i,m}_{\mathrm{DC}}$, illuminance lower and upper bounds E^l_k and E^u_k, ambient lighting level E^{Am}_k, $c^*_r = -\infty$, $\kappa = 1$, $z^l = -\infty$, and $z^u = \infty$.

Output: Time fraction (out of one time unit) ω_q and solution of the RMP z^u.

1. Compute $P_{\mathrm{AC,Avg}}(\mathcal{I}_q)$ and $P_{\mathrm{DC}}(\mathcal{I}_q)$ for $\tilde{\mathcal{Q}}$, and compute $P^{\min}_{\mathrm{illumi}}$;
2. **while** $z^u/z^l > 1+\epsilon$ and $c^*_r < 0$ **do**
3. solve the RMP and obtain its optimal result z^u and dual optimal solution λ_j;
4. solve the PP with λ_j and obtain an IS $\mathcal{I}_q$ with c^*_r and the corresponding optimal $P^{i,q,m}_{\mathrm{DC}}$;
5. update c^*_r and $\tilde{\mathcal{Q}} = \tilde{\mathcal{Q}} \cup \mathcal{I}_q$ and compute the new $P_{\mathrm{AC,Avg}}(\mathcal{I}_q)$ and $P_{\mathrm{DC}}(\mathcal{I}_q)$;
6. $z_l = z^u + c^*_r$;
7. end while
8. update the link capacity in the RMP by reality check;
9. solve the constraint-updated RMP and obtain its optimal result z^u.

VI. Practical Issues

A. Three Configurations of the Light Source

Typically, a light source operates with a fixed beam angle (i.e., formed by the central luminous flux and the central vertical line) and beam width (i.e., semi-angle at half-power $\theta_{1/2}$). This configuration is capable of efficiently providing sufficient illumination. However, its weak competitiveness manifests on the communication functionality due to the high interlink interference and nonuniform distribution of optical signal strength, which will lead to severe degradation of channel gain when the transceivers are not strictly aligned. To mitigate the interference and enhance the channel gain, mechanically steering the beam angle and beam width is introduced in [15] and [12]. In this paper, we further explore the impact of tuning the beam angle and beam width on the power consumption of multiuser VLC indoor networks. Although an adjustable beam angle can be implemented by the traditional *mechanical steering* method, the energy cost of tuning the orientation of the light source is considerable [19], and, even worse, the time it takes to change the direction is inevitable, which will cause a significant negative impact on the network delay and capacity. To circumvent these problems, a new structure of the light source is proposed. Multiple chips with different beam angles and beam widths are installed on one light source and the diversity of orientation of the light source can be implemented by activating any of those chips. This configuration is motivated by the "electronic steering" concept introduced in [19]. Because the new structure of the light source needs to be specified before being evaluated by the optimization algorithm, we outline an implementable design of such a light source based on the assumption of uniformly distributed UTs. In summary, three configurations[1] (shown in Fig. 3) of the light source are investigated: (1) fixed beam angle and beam width, (2) mechanically adjustable beam angle and beam width, and (3) electronically selectable beam angle and beam width.

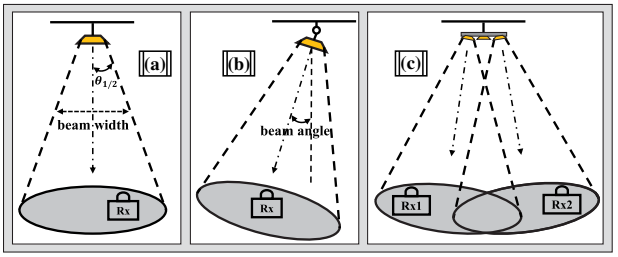

Fig. 3. Three different configurations: (a) fixed beam angle and beam width, (b) mechanically adjustable beam angle and beam width, and (c) electronically selectable beam angle and beam width.

As shown in Fig. 3, for Configuration a, the beam width and beam angle are fixed regardless of the location of the UT. The orientation of all VLC APs are vertical to the horizontal UT plane. The semi-angle at half-power $\theta_{1/2}$ (i.e., beam width) of AC and DC powered sources are the same. For Configuration b, the beam width and beam angle are tunable. For the purpose of concentrating the optical signal, the $\theta_{1/2}$ of the AC powered source is set to be smaller than that of the DC powered source. By adjusting the beam angle, the transmitter can directly point to the receiver. It can be seen that, for Configuration b, the radiance angle of each link is always zero. For Configuration c, multiple chips are installed on one VLC AP. The beam angle and beam width of each chip are fixed. Nevertheless, the VLC AP can selectively activate any of those chips and "electronically steer" the beam angle and beam width. Note that, because the beam angle of each chip (for Configuration c) is fixed, the transmitter might not be able to directly point to the receiver, such as for Configuration b. Next, we specify the new structure of the light source for Configuration c.

[1]In order to distinguish the difference among three configurations, it is assumed that, in the first and the second configurations, the beam angles of all the transmitters on one VLC AP are the same.

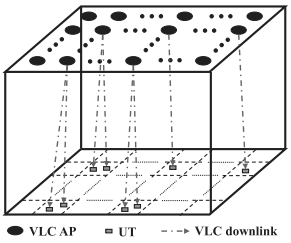

Fig. 4. Grid structure of multiuser VLC indoor network.

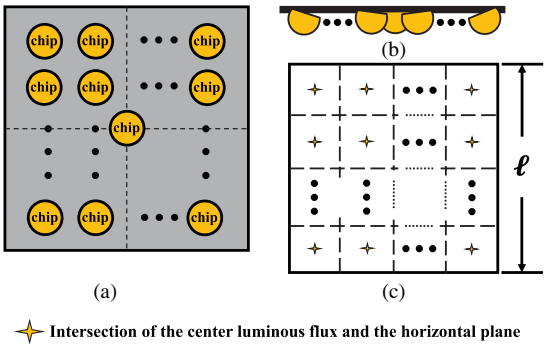

Fig. 5. New structure of the light source. (a) Top view: one central chip and $n \times n$ peripheral chips. (b) Left view. (c) Served square area of a VLC AP.

B. New Structure of the Light Source

As shown in Fig. 4, the VLC APs are mounted on the ceiling in a grid structure. To maximize the capacity of each link, each UT[2] chooses the nearest VLC AP to associate with; thus, the served area of each VLC AP can be modeled as a square. In Fig. 5, a new structure of the light source is shown. It can be seen in Fig. 5(a) that one VLC AP is equipped with $(n \times n) + 1$ chips, including $n \times n$ (n is a multiple of 2) peripheral chips and one central chip, which is mainly responsible for illuminating. In Fig. 5(c), a square area served by a VLC AP is equally divided into $n \times n$ small square regions. Each peripheral chip is assigned to serve the closest small square region. The star (i.e., center of coverage) in each region is the intersection of the central luminous flux of the corresponding peripheral chip and the horizontal UT plane. Each star is located at the center of each square region. Given the location of a star and the height of the room, the beam angle of the corresponding chip can be determined. Denote the side length of a square area served by a VLC AP as l, the maximum distance $d_{\max}$ between a UT and its corresponding center of coverage satisfy $d_{\max} \le \frac{\sqrt{2}l}{2n}$. We understand that the electronic steering VLC AP increases the price of the light source. However, this installation fee is a one-time cost, and, in contrast, the energy saving performance, which will be shown later in the numerical analysis, is beneficial for the entire life cycle. In addition, according to the reports and forecasts [39,40], the LED's price has dropped significantly in recent years and is also expected to keep declining. This means that the new light source configuration could actually be cost-efficient.

[2]To focus on the configuration of the light source and make it easier to understand, it is assumed here and also in the simulation that each UT is equipped with only one receiver. It means that each UT can connect to only one VLC AP at a time.

C. Constructing the Conflict Graph

In this section, we also introduce an effective approach to constructing the conflict graph for multiuser VLC indoor networks. Traditionally, in the protocol model, whether or not a transmission is being interfered by another transmission is determined by the distance between the receiver and the nonintended transmitter [32,38,41]. In the VLC network, this standard is not always applicable because the optical signal propagation may not be isotropic from the perspective of the UT plane. In [13], the orientation of each VLC AP is fixed and vertical to the horizontal UT plane, such that the conflict graph, constructed by using the interference range [32] as in RF networks, is valid. However, if the orientation of VLC APs is tunable, then the interference range is not a reliable measure to accurately model the level of interference. As shown in Fig. 6, in case a, the receiver of link 2 is outside the interference range of link 1; thus, the transmission of link 1 will not produce non-negligible interference to link 2. However, in case b, because the beam angle of link 1 is changed, even though the receiver of link 2 is outside the conventional distance-based interference range of link 1, the data transmission of link 2 may be disrupted by that of link 1. As such, we propose a new criterion, according to which, if one of the pairwise signal-to-interference ratio (SIR) measurements of two links is lower than a threshold $\mathrm{SIR}_{\mathrm{th}}$, those two links cannot be scheduled in the same IS.

Under the protocol model, we define a maximum SIR threshold as $\mathrm{SIR}_{\mathrm{th}}^{\max}$ such that, if $\mathrm{SIR}_{\mathrm{th}} \ge \mathrm{SIR}_{\mathrm{th}}^{\max}$, then, when any link is active, other links on the same channel cannot be active. A minimum SIR threshold $\mathrm{SIR}_{\mathrm{th}}^{\min}$ is 1 because, if $\mathrm{SIR}_{\mathrm{th}} < 1$, the interference signal will be stronger than the transmission signal. For a wireless network with high traffic load, there could exist an upper-bound $\mathrm{SIR}_{\mathrm{th}}^{U}$ for the SIR threshold such that if $\mathrm{SIR}_{\mathrm{th}} > \mathrm{SIR}_{\mathrm{th}}^{U}$, the protocol model solution is infeasible (i.e., $\sum_{1 \le q \le |\mathcal{Q}|} \omega q > 1$). For a dense wireless network, there could exist a lower-bound $\mathrm{SIR}_{\mathrm{th}}^{L}$ such that, if $\mathrm{SIR}_{\mathrm{th}} < \mathrm{SIR}_{\mathrm{th}}^{L}$, even though the protocol model solution is feasible (i.e., $\sum_{1 \le q \le |\mathcal{Q}|} \omega q \le 1$), the reality check

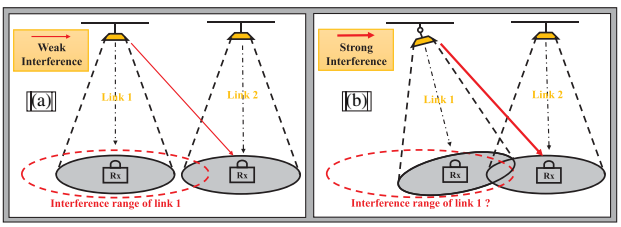

Fig. 6. Example of the shortcoming of the conventional interference range.

result is infeasible. Therefore, we need to select the $\mathrm{SIR}_{\mathrm{th}}$ within the range $[\mathrm{SIR}_{\mathrm{th}}^{L}, \mathrm{SIR}_{\mathrm{th}}^{U}]$. In the next section, we study the $\mathrm{SIR}_{\mathrm{th}}^{U}$ and the $\mathrm{SIR}_{\mathrm{th}}^{L}$ for a VLC indoor network with three different configurations of light source through simulations.

VII. Numerical Results

In this section, we conduct extensive simulations to evaluate our proposed algorithm integrated with the practical issues. The simulations are conducted under MATLAB R2013b and CPLEX 12.6.1 [42] on a computer with 2.0 GHz and 4 GB RAM. We study the cost of solving the MP under different values of ϵ. Our proposed algorithm is compared with two other recent schemes [12,13] in terms of power consumption and running time. In [12], the VICO framework does not consider the illumination constraints in the algorithm. Let P_{total} represent the total power consumption of a given scheme; because the illumination is always needed, the power consumption evaluated in the numerical analysis is $P_{\mathrm{total}} - P_{\mathrm{illumi}}^{\mathrm{min}}$.

The room size is 6.0 m × 6.0 m × 3.0 m. The desk height is 0.8 m, and the UTs are randomly distributed on the desk according to uniform distribution. There are 36 (6 × 6) VLC APs in the grid structure installed on the ceiling, and each VLC AP is equipped with one chip[3] (i.e., transmitter) filled with 625 (25 × 25) white light LEDs. Note that, for the new structure of the light source (Fig. 7), each VLC AP is equipped with five such chips.[4] The distances between two neighboring VLC APs and two neighboring LEDs are 1 m and 1 cm, respectively. Therefore, the size of each small square region is 0.5 m × 0.5 m. Given that the height of the room and the desk are 3 and 0.8 m, respectively, the beam angle of each chip can be estimated by $\arctan\left(\frac{0.25\sqrt{2}}{3-0.8}\right)$. The maximum transmitted optical power of each LED is 20 mW. The value of P_{AC} of each VLC AP is set to 0.1 W. $P_{\mathrm{AC,Avg}}$ is set to be half of P_{AC}. The channel bandwidth of each VLC link is 100 MHz, and we assume all the VLC APs use the same channel in the simulation. The constant Gaussian noise is calculated from the parameters in [29] and set to be 4.7×10^{-14} A^2. The receiver parameters (i.e., the FOV of the receiver, the detector area of a photodiode, the gain of the optical filter, the refractive index of the lens, and the O/E conversion efficiency) are the same as those in [29]. The required illuminance range is 300–500 lux. For Configuration a, the semi-angle at half power $\theta_{1/2}$ of the AC and DC powered sources are both set to 70°. For Configuration b, $\theta_{1/2}$ of the AC powered source is set to 30°, while that of the DC powered source is set to 70°. For Configuration c, as shown in Fig. 7, $\theta_{1/2}$ of the central chip is set to 70°, and $\theta_{1/2}$ of the peripheral chips are all set to 30°. The wall plug efficiency factors η_{AC} and η_{DC} for all the VLC transmitters are set to 0.02 and 0.1, respectively.

[3]This means that each VLC AP can serve only one UT at a time.

[4]In order to fairly evaluate the three configurations, for Configuration c, it is assumed that only one of the peripheral chips can be active for data transmission at a time, and the total optical power generated from one VLC AP cannot exceed the P_{max} of a single chip.

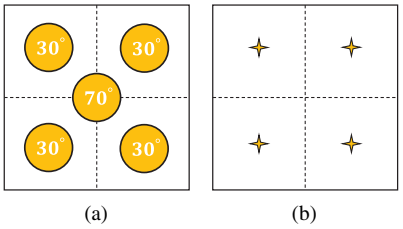

Fig. 7. Sample of the new structure of the light source. (a) Top view of the sample VLC AP. (b) Served square area of the sample VLC AP.

A. Cost of Solving the MP

For a 30 UT VLC indoor network, Table II shows the number of iterations and the total running time needed to achieve a ϵ-bounded solution. It can be seen that it takes 14 iterations and 9.33 s to obtain 1% bounded results, and 44 iterations and 17.84 s to obtain a near-optimal result (i.e., $\epsilon \approx 0$). As the technique of computation evolves, particularly the parallel computing, the overhead of the algorithm is expected to reduce further. For nomadic situations, compared with the period during which the network pattern remains fixed, the running time for finding the ϵ-bounded solution is very short. For the following numerical results, we use $\epsilon = 0.01$.

B. Constructing Conflict Graph

For a 30 UT VLC indoor network under Configuration a, the traffic demand of each UT is 20 Mbps, we show the protocol model solutions and the corresponding reality check results in Fig. 8. The upper bound for SIR threshold $\mathrm{SIR}_{\mathrm{th}}^{U}$

TABLE II
Iteration Number and Running Time for an ϵ-Bounded Solution

ϵ	Number of Iterations	Running Time (s)
0.01	14	9.33
0.005	22	11.56
1×10^{-14}	44	17.84

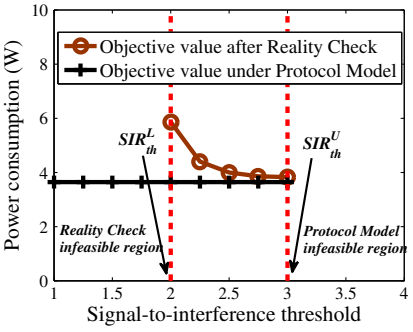

Fig. 8. Protocol model solutions and corresponding reality check results.

is 3, and if $\mathrm{SIR}_{\mathrm{th}} > 3$, the protocol model solution will be infeasible. The lower bound for SIR threshold $\mathrm{SIR}_{\mathrm{th}}^{L}$ is 2, and, if $\mathrm{SIR}_{\mathrm{th}} < 2$, the reality check solution will be infeasible. When $2 \le \mathrm{SIR}_{\mathrm{th}} \le 3$, although the protocol model solution is almost the same, a lower $\mathrm{SIR}_{\mathrm{th}}$ will lead to a higher reality check result, which is due to neglecting the nonzero interference in the protocol model. Thus, choosing $\mathrm{SIR}_{\mathrm{th}}^{U}$ as the SIR threshold will minimize the total power consumption while satisfying the traffic demands. We also conduct simulations for a 60 UT (each UT requires 20 Mbps) indoor VLC network under Configuration c, to compare the performance of SIR threshold based and conventional distance based conflict graph modeling. As shown in Fig. 9, the minimum power consumption achieved by the SIR threshold approach is around 7 W, while that achieved by the distance threshold approach is around 12 W.

In Fig. 10, we show the $\mathrm{SIR}_{\mathrm{th}}^{U}$ and the $\mathrm{SIR}_{\mathrm{th}}^{L}$ for a VLC indoor network under the three configurations. As the number of UTs increases, the $\mathrm{SIR}_{\mathrm{th}}^{U}$ will decrease and the $\mathrm{SIR}_{\mathrm{th}}^{L}$ will increase. And, when the $\mathrm{SIR}_{\mathrm{th}}^{U}$ and the $\mathrm{SIR}_{\mathrm{th}}^{L}$ converge to one value, this indicates that the traffic load reaches up to the system capacity. From Fig. 10, we can observe that the system capacity of Configurations b and c is around double that of Configuration a. And the feasible region of Configuration b and c is larger than that of Configuration a, which shows the superiority of the new structure of the light source (i.e., Configuration c).

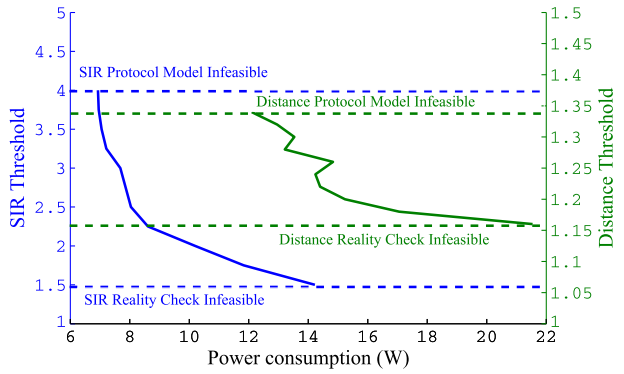

Fig. 9. SIR threshold versus distance threshold.

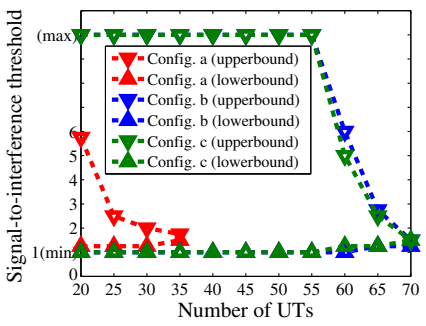

Fig. 10. $\mathrm{SIR}_{\mathrm{th}}^{L}$ and $\mathrm{SIR}_{\mathrm{th}}^{U}$ for three configurations.

C. Power Consumption Evaluation

In the following, we evaluate the objective value (i.e., power consumption) for the three configurations, in terms of different number of UTs. Figure 11 shows that the real power consumption (after reality check) for Configuration a is more than double that for Configuration b and c. More to the point, the real power consumption for Configuration c, which is much more practical than Configuration b, is almost the same as that for Configuration b. In summary, the new structure of the light source (i.e., Configuration c) is a practical design and will provide excellent power-saving performance.

We also compare the ϵ-bounded solution obtained by column generation (CG) with the results obtained by a random link scheduling introduced in VICO [12] and a link scheduling based on the maximum weighted independent set (MWIS) introduced in [13]. The real power consumption under the three algorithms are simulated in terms of a different number of UTs and a different throughput requirement of each UT. As shown in Fig. 12, the traffic demand of each UT is 5 Mbps, the real power consumption under VICO and the MWIS becomes much higher than that under CG, as the number of UTs increases. For a 35 UT network, the CG algorithm cuts the power consumption of VICO by 60%. Although the MWIS algorithm can achieve a better objective value under the protocol model than random scheduling, after reality check its power consumption is much

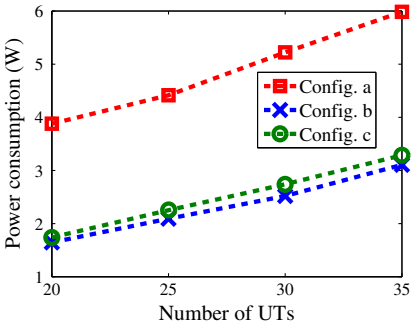

Fig. 11. Real power consumption under a different number of UTs for the three configurations.

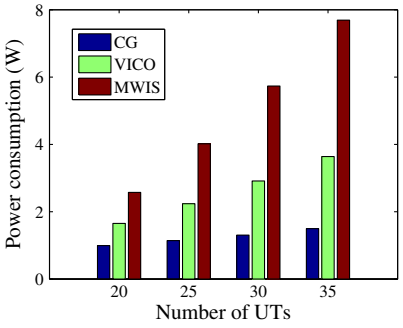

Fig. 12. Real power consumption under a different number of UTs for the three algorithms.

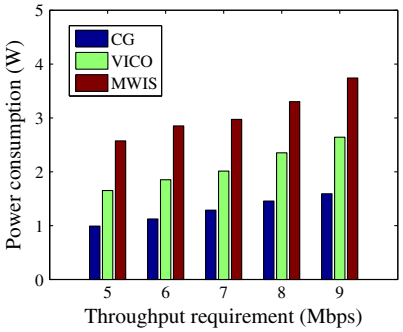

Fig. 13. Real power consumption under a different throughput requirement for the three algorithms.

worse than that of VICO due to neglecting the nonzero interference from other links. The results shown in Fig. 13 are consistent with the above analysis. For a 20 UT VLC network, as the throughput requirement of each UT increases, there are almost no changes in the gaps between the real power consumption obtained by the three algorithms.

D. Illumination Evaluation

Regarding the illuminance satisfaction, in our proposed algorithm, because the illuminance level for the entire horizontal space is conditioned to be within the specified range (300–500 lux), the illuminance distribution always meets the requirements. In Fig. 14, we show a sample distribution of illuminance under our proposed algorithm. We also show a sample illuminance distribution under the VICO framework in Fig. 15. Around 70% of the horizontal space does not meet the illumination requirements because the VICO framework does not take the illumination constraints into account when performing the optimization algorithm.

E. Cost of the Three Algorithms

The running time costs by minimizing the power consumption under the three algorithms are shown in Fig. 16. We can observe that the CG algorithm costs around 5.2 s more than that of the random link scheduling under VICO. Nevertheless, the optimization algorithm can be run

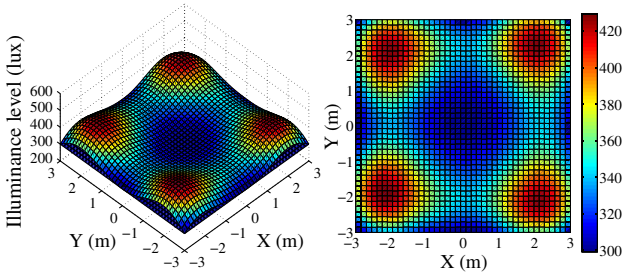

Fig. 14. Sample distribution of illuminance created by our proposed algorithm with the entire horizontal space illumination constraints.

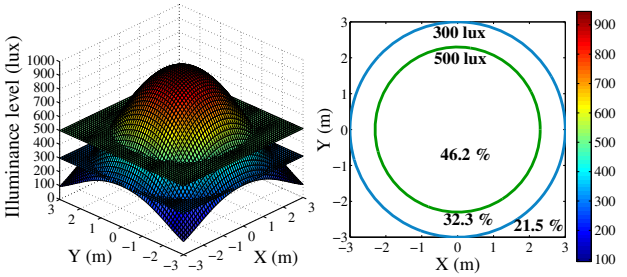

Fig. 15. Sample distribution of illuminance under the VICO framework.

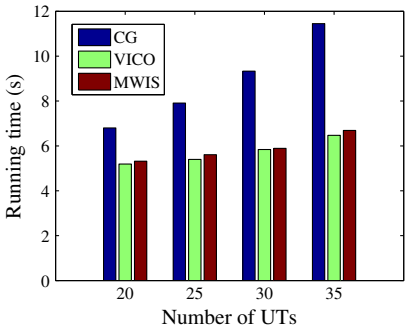

Fig. 16. Algorithm running time under a different number of UTs for the three algorithms.

with a one-time cost in the centralized controller and no extra operations are needed until the network environment changes. This extra overhead is acceptable, given that our algorithm can achieve a 60% power-saving performance while satisfying the illumination requirements.

VIII. Conclusion

In this paper, we investigate the problem of minimizing the total power consumption of a general multiuser VLC indoor network while satisfying the traffic demands and providing an acceptable level of illumination. A column-generation-based ϵ-bounded algorithm with reality check is proposed. Regarding the light source, three configurations are considered and one of them (i.e., a new structure of the light source) is proposed. For constructing the conflict graph, an effective range of the SIR threshold is evaluated by extensive simulation results. The power consumption of the three configurations are evaluated by simulations and the results reveal that the new structure of the light source is practical and provides power-efficient solutions. Compared with two other VLC link scheduling algorithms, our proposed algorithm can achieve a better performance of power consumption, especially in crowded scenarios, while satisfying the illumination requirements on the entire horizontal plane.

Acknowledgment

This work was supported in part by the National Science Foundation (NSF) grant ECCS-1331018.

References

[1] Cisco, "Cisco visual networking index: Forecast and methodology, 2014–2019," Cisco White Paper, 2015.

[2] Ericsson, "Optimizing the indoor experience," 2013 [Online]. Available: http://www.ericsson.com/res/docs/2013/real-performance-indoors.pdf.

[3] Alcatel-Lucent, "In-building wireless: One size does not fit all," 2015 [Online]. Available: https://www.alcatel-lucent.com/solutions/in-building/in-building-infographic.

[4] Cisco, "Cisco Service Provider Wi-Fi: A platform for business innovation and revenue generation," 2015 [Online]. Available: http://www.cisco.com/c/en/us/solutions/collateral/service-provider/service-provider-wi-fi/solution_overview_c22-642482.html.

[5] Cisco, "Global mobile data traffic forecast update, 2014–2019," Cisco White Paper, 2015.

[6] S. Chia, M. Gasparroni, and P. Brick, "The next challenge for cellular networks: Backhaul," *IEEE Microwave Mag.*, vol. 10, no. 5, pp. 54–66, 2009.

[7] S. Tsuzuki, I. S. Areni, and Y. Yamada, "A feasibility study of 1 Gbps PLC system assuming a high-balanced DC power-line channel," in *16th IEEE Int. Symp. on Power Line Communications and Its Applications (ISPLC)*, 2012, pp. 386–391.

[8] A. M. Tonello, P. Siohan, A. Zeddam, and X. Mongaboure, "Challenges for 1 Gbps power line communications in home networks," in *IEEE 19th Int. Symp. on Personal, Indoor and Mobile Radio Communications (PIMRC 2008)*, 2008, pp. 1–6.

[9] C. M. Lonvick, C. Duffy, L. O. Suau, D. Schriner, and M. A. Laherty, "Controlling intelligent powered devices," U.S. patent 20,150,301,544 (Oct. 22, 2015).

[10] D. Hanchard, "FCC chairman forecasts wireless spectrum crunch," 2010 [Online]. Available: http://www.zdnet.com/article/fcc-chairman-forecasts-wireless-spectrum-crunch/

[11] X. Deng, Y. Wu, K. Arulandu, G. Zhou, and J.-P. M. Linnartz, "Performance comparison for illumination and visible light communication system using buck converters," in *GLOBECOM Workshops*, 2014, pp. 547–552.

[12] Y. Li, L. Wang, J. Ning, K. Pelechrinis, S. V. Krishnamurthy, and Z. Xu, "VICO: A framework for configuring indoor visible light communication networks," in *IEEE 9th Int. Conf. on Mobile Ad Hoc and Sensor Systems (MASS)*, 2012, pp. 136–144.

[13] Y. Tao, X. Liang, J. Wang, and C. Zhao, "Scheduling for indoor visible light communication based on graph theory," *Opt. Express*, vol. 23, no. 3, pp. 2737–2752, 2015.

[14] I. Din and H. Kim, "Energy-efficient brightness control and data transmission for visible light communication," *IEEE Photon. Technol. Lett.*, vol. 26, no. 8, pp. 781–784, 2014.

[15] D. Tronghop, J. Hwang, S. Jung, Y. Shin, and M. Yoo, "Modeling and analysis of the wireless channel formed by LED angle in visible light communication," in *Int. Conf. on Information Networking (ICOIN)*, 2012, pp. 354–357.

[16] X. Li, R. Zhang, and L. Hanzo, "Cooperative load balancing in hybrid visible light communications and Wi–Fi," *IEEE Trans. Commun.*, vol. 63, no. 4, pp. 1319–1329, 2015.

[17] D. Wu, Z. Ghassemlooy, W.-D. Zhong, and C. Chen, "Cellular indoor OWC systems with an optimal Lambertian order and a handover algorithm," in *7th Int. Symp. on Telecommunications (IST)*, 2014, pp. 777–782.

[18] M. Rahaim and T. D. Little, "SINR analysis and cell zooming with constant illumination for indoor VLC networks," in *2nd Int. Workshop on Optical Wireless Communications (IWOW)*, 2013, pp. 20–24.

[19] B. Nakhkoob, M. Bilgi, M. Yuksel, and M. Hella, "Multi-transceiver optical wireless spherical structures for MANETs," *IEEE J. Sel. Areas Commun.*, vol. 27, no. 9, pp. 1612–1622, 2009.

[20] H. Sugiyama, S. Haruyama, and M. Nakagawa, "Brightness control methods for illumination and visible-light communication systems," in *3rd Int. Conf. on Wireless and Mobile Communications (ICWMC)*, 2007, p. 78.

[21] Z. Huang and Y. Ji, "Design and demonstration of room division multiplexing-based hybrid VLC network," *Chin. Opt. Lett.*, vol. 11, no. 6, 060603, 2013.

[22] N. Ding, D. Wagner, X. Chen, A. Pathak, Y. C. Hu, and A. Rice, "Characterizing and modeling the impact of wireless signal strength on smartphone battery drain," *ACM SIGMETRICS Perform. Eval. Rev.*, vol. 41, no. 1, pp. 29–40, 2013.

[23] S. Shao, A. Khreishah, M. B. Rahaim, H. Elgala, M. Ayyash, T. D. Little, and J. Wu, "An indoor hybrid Wi–Fi-VLC Internet access system," in *IEEE 11th Int. Conf. on Mobile Ad Hoc and Sensor Systems (MASS)*, 2014, pp. 569–574.

[24] S. Shao, A. Khreishah, M. Ayyash, M. B. Rahaim, H. Elgala, V. Jungnickel, D. Schulz, T. D. Little, J. Hilt, and R. Freund, "Design and analysis of a visible-light-communication enhanced Wi–Fi system," *J. Opt. Commun. Netw.*, vol. 7, no. 10, pp. 960–973, 2015.

[25] S. Shao, A. Khreishah, M. Ayyash, M. B. Rahaim, H. Elgala, V. Jungnickel, D. Schulz, and T. D. C. Little, "Design of a visible-light-communication enhanced WiFi system," arXiv:1503.02367v2, 2015.

[26] M. Ayyash, H. Elgala, A. Khreishah, V. Jungnickel, T. Little, S. Shao, M. Rahaim, D. Schulz, J. Hilt, and R. Freund, "Coexistence of WiFi and LiFi towards 5G: Concepts, opportunities, and challenges," *IEEE Commun. Mag.*, vol. 54, no. 2, pp. 64–71, 2015.

[27] S. Shao, A. Khreishah, and I. Khalil, "Joint link scheduling and brightness control for greening VLC-based indoor access networks," arXiv:1510.00026, 2015.

[28] T.-H. Hsu, "Optimization on color characteristics for LED lighting system," Master's thesis, National Central University, Taiwan, p. 51, 2005.

[29] T. Komine and M. Nakagawa, "Fundamental analysis for visible-light communication system using LED lights," *IEEE Trans. Consum. Electron.*, vol. 50, no. 1, pp. 100–107, 2004.

[30] J. Zhang, X. Zhang, and G. Wu, "Dancing with light: Predictive in-frame rate selection," in *IEEE INFOCOM*, 2015, pp. 1–9.

[31] K.-D. Langer, J. Hilt, D. Shulz, F. Lassak, F. Hartlieb, C. Kottke, L. Grobe, V. Jungnickel, and A. Paraskevopoulos, "Rate-adaptive visible light communication at 500 Mb/s arrives at plug and play," SPIE Newsroom, 2013.

[32] P. Gupta and P. R. Kumar, "The capacity of wireless networks," *IEEE Trans. Inf. Theory*, vol. 46, no. 2, pp. 388–404, 2000.

[33] R. Diestel, *Graph Theory*, Graduate Texts in Mathematics. Springer, 2005.

[34] T. M. Cover and J. A. Thomas, *Elements of Information Theory*. Hoboken, NJ: Wiley, 2012.

[35] I. Stefan and H. Haas, "Hybrid visible light and radio frequency communication systems," in *IEEE 80th Vehicular Technology Conf. (VTC Fall)*, 2014, pp. 1–5.

[36] D. Bertsimas and J. N. Tsitsiklis, *Introduction to Linear Optimization*. Athena Scientific, 1997.

[37] J. Desrosiers and M. E. Lübbecke, *A Primer in Column Generation*. New York, NY: Springer, 2005.

[38] Y. Shi, Y. T. Hou, J. Liu, and S. Kompella, "Bridging the gap between protocol and physical models for wireless networks," *IEEE Trans. Mobile Comput.*, vol. 12, no. 7, pp. 1404–1416, 2013.

[39] A. Parker, "LED price-performance," 2014 [Online]. Available: http://www.digitallumens.com/?attachment_id=2795.

[40] J. Carbone, "LED market grows as prices decline," 2011 [Online]. Available: http://www.digikey.com/en/articles/techzone/2011/jan/led-market-grows-as-prices-decline.

[41] Y. Shi and Y. T. Hou, "Optimal power control for multi-hop software defined radio networks," in *26th IEEE Int. Conf. on Computer Communications (INFOCOM)*, 2007, pp. 1694–1702.

[42] I. ILOG, "CPLEX optimizer, version 12.6.1," 2014 [Online]. Available: http://www-03.ibm.com/software/products/de/ibmilogcpleoptistud/.

Sihua Shao received his B.S. degree in electrical and information engineering from South China University of Technology in 2011, and his M.S. degree in electrical and information engineering from Hong Kong Polytechnic University in 2012. He is currently a Ph.D. student in the Department of Electrical and Computer Engineering at New Jersey Institute of Technology. His current research interests include wireless communication, visible light communication, and heterogeneous networks. He is a student member of the IEEE.

Abdallah Khreishah received his Ph.D. and M.S. degrees in electrical and computer engineering from Purdue University in 2010 and 2006, respectively. Prior to that, he received his B.S. degree with honors from Jordan University of Science and Technology in 2004. During the last year of his Ph.D., he worked with NEESCOM. He is currently an assistant professor in the ECE department of New Jersey Institute of Technology. His research spans the areas of green communications and networking, visible-light communications, wireless networks, and network security. His research projects are funded by the National Science Foundation, New Jersey Department of Transportation, and the UAE Research Foundation.

Issa Khalil received B.Sc. and M.Sc. degrees from Jordan University of Science and Technology in 1994 and 1996 and a Ph.D. degree from Purdue University, USA, in 2006, all in computer engineering. Immediately thereafter he worked as a post-doctoral researcher in the Dependable Computing Systems Lab of Purdue University until he joined the College of Information Technology (CIT) of the United Arab Emirates University (UAEU) in August 2007. In September 2011, Dr. Khalil was promoted to associate professor and served as the department chair of the Information Security Department in CIT. In June 2013, Dr. Khalil joined the Cyber Security Group at the Qatar Computing Research Institute (QCRI), a member of the Qatar Foundation, as a senior scientist. Dr. Khalil's research interests span the areas of wireless and wireline network security and privacy. He is especially interested in cloud security, botnet detection and takedown, and security data analytics. Dr. Khalil served as the technical program co-chair of the 6th International Conference on Innovations in Information Technology and was appointed as a technical program committee member and reviewer for many international conferences and journals. In June 2011, Dr. Khalil was granted the CIT outstanding professor award for outstanding performance in research, teaching, and service.